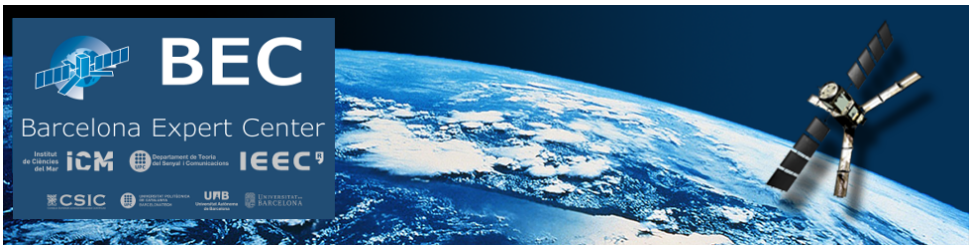

File: BEC-SMOS-0004-PD-SSS-ARCTIC.pdf, version 1.0

Title: SMOS-BEC ARCTIC Region SSS Product Description.

Authors: BEC Team.

Contact: smos-bec@icm.csic.es

Date: 19/06/2019

SMOS-BEC ARCTIC REGION SSS PRODUCT DESCRIPTION

Abstract: This technical note describes the retrieval of L3 SMOS SSS for the Arctic and Sub-Arctic regions distributed by the BEC team through its data visualization and distribution service http://bec.cmima.csic.es

Contents

1 INTRODUCTION

This technical note aims to present and assess the quality of seven years (2011-2017) of 25 km 9-day SMOS SSS objectively analyzed maps in the Arctic and sub-Arctic oceans (50^oN-90^oN). The SMOS SSS maps presented here are an improved version of the preliminary three-years data set generated and freely distributed by the Barcelona Expert Center. In this new version (v2.0), a time-dependent bias correction has been applied to mitigate the seasonal bias that affected the previous SSS maps. An extensive data base of *in-situ* data (Argo floats and thermosalinograph measurements) has been used for assessing the accuracy of this product. The standard deviation of the difference between the new SMOS SSS maps and Argo SSS ranges from 0.25 and 0.35. The major features of the interannual SSS variations observed by the thermosalinographs are also captured by the SMOS SSS maps. However, the validation in some regions of the Arctic Ocean has not been feasible because of the lack of *in-situ* data. In those regions, qualitative comparisons with SSS provided by models and the remotely sensed SSS provided by Aquarius and SMAP have been performed. Despite the differences between SMOS and SMAP, both data sets show consistent SSS variations with respect to the model and the river discharge *in-situ* data, but present a larger dynamic range than that of the model. This result suggests that, in those regions, the use of the remotely sensed SSS may help to improve the models.

2 SCIENCE ALGORITHM OVERVIEW

2.1 Level 2 Algorithms

The debiased non-Bayesian retrieval of SSS introduced in [Olmedo et al., 2017] aims to correct two known issues: the systematic biases caused by the presence of land masses and radio interference, and the data gaps due to the non-convergence of the retrieval algorithm.

2.1.1 Input data

The Brightness temperatures (TBs) obtained from SMOS MIRAS L1B TBs v620 provided by ESA are used as an input for the SMOS SSS retrieval. The L1B v620 product contains the Fourier coefficients of the measured brightness temperature. Starting from this product, using ESA's Earth Observation Customer Furnished Item (EOCFI) orbit propagation libraries [ESA, 2014] and following a similar procedure as the one used in the operational SMOS level 1 processor chain [Deimos, 2014], the measured TBs are obtained in the antenna reference frame (ARF). The unique difference from the standard processor is the number of points contained per snapshot (*i.e.* the resolution). The operational processor uses, at antenna level, a hexagonal grid of 128×128 points (*i.e.* $2^7 \times 2^7$). The projection of this antenna grid into the ground provides a resolution of about 15 km at bore-sight. This resolution is more than twice SMOS theoretical finer resolution [McMullan et al., 2008]. We have thus reduced the computational cost without actually losing information by using an antenna hexagonal grid of 64×64 ($2^6 \times 2^6$) points.

2.1.2 Forward Model

The forward model linking the modeled TB to SSS relies on the dielectric constant model proposed by Meissner and Wentz [Meissner and Wentz, 2004] which non-linearly depends on SSS and SST. Nevertheless, the measured TB not only contains information about brightness temperature of the flat sea, but also contributions due to other main sources: the roughness of the sea surface [Guimbard et al., 2012], the reflected emission of the atmosphere, the reflection on the sea surface of the galactic emission ([Tenerelli et al., 2008]) and the sun glitter [Reul et al., 2007]. Therefore, all these additional contributions to the TB(θ_j, SSS, p_1, . . . , p_{Np}) term must be modeled at the bottom of the atmosphere (BOA) and then translated to the ARF prior to minimizing Eq. (1). Thus, the atmospheric attenuation effect over brightness temperature must be taken into account together with the direct emission of the atmosphere itself to estimate the modeled TB at the top of the atmosphere (TOA). Finally, to go from TOA to ARF, the ionosphere must be taken into account. The ionospheric effect translates into a rotation in the polarization components of TB. All these contributions are described in detail in Ocean SMOS Team (2016).

2.1.3 Non-Bayesian retrieval of SSS

We retrieve a single SSS value for each TB measurement, that is, along the same dwell line we have a value of SSS for each valid incidence angle, namely:

$$F^{j}_{non-Bayesian}(SSS) = \left[I^{meas}(\theta_j) - I(\theta_j, SSS, p_1, \ldots, p_{N_p})\right]^2, \quad (1)$$

where the super index j indicates one of the N_m available incidence angles. The term $I = (TB_v + TB_h)/2$, both for the forward modeled (section 2.1.2) and measured data, is the First Stokes parameter at BOA divided by 2; by summing up vertical (TB_v) and horizontal (TB_h) polarization we obtain a

term which is independent from Faraday rotation and simplifies its processing, although the retrieval could be done with each polarization independently. For the optimization, the other geophysical variables are given a fixed value, that of the geophysical priors p_k^0.

2.1.4 SSS spatial bias characterization: definition of a SMOS-based climatology

The characterization of bias is based on a classification of the non-Bayesian single-angle salinities retrieved using eq. (1). A first geophysical consistency filter on non-Bayesian salinities is applied: we discard any value out of the range $[0, 50]$. Then, the single-angle SSS values are grouped together according to their geolocation (latitude and longitude in a cylindrical grid of $0.25^o \times 0.25^o$, φ and λ), overpass direction (ascending or descending, denoted by a binary variable d), across-track distance to the center of swath (in 50-km bins, denoted by x) and incidence angle (in 5° bins, denoted by θ). For each given 5-tuple, $c = (\varphi, \lambda, d, x, \theta)$, we take all the retrievals $\{SSS(\varphi, \lambda, d, x, \theta)\}$ in the period we use (2011 to 2016) and construct the associated histograms (see Figure 1). The choice of the parameters used in the definiton of the tuple is further detailed in [Olmedo et al., 2017] (section 2.2.2).

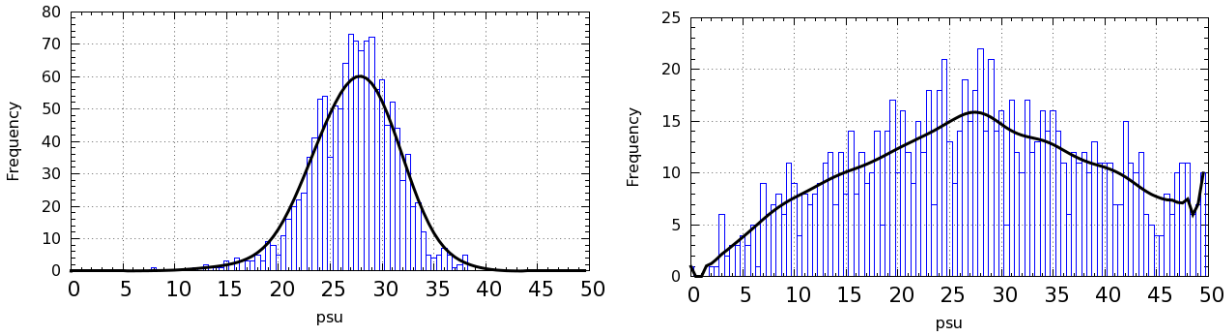

Figure 1: SMOS SSS histogram associated with $c = (20, -29, A, 225, 52)$ (left) and to $c = (31, 133, A, 275, 47)$ (right) (see the text for more details).

For every tuple, the corresponding SSS histogram is defined with bins of 0.5 psu. In order to improve the accuracy of the histogram and minimize the dependency on the histogram discretization, the mean of SSS inside each bin is considered as the representative value of SSS on that bin. The mode of the histograms are taken as a measure of the central reference value; the advantage of taking the mode, instead of other statistics, is that the mode is unaffected by the presence of outliers or by the skewness of the distribution.

The accuracy of the estimation of the mode of any histogram is relatively low, mainly because of the lack of sampling. To overcome this issue we have applied three times a weighted averaging window (with a size of seven points, including the central point, the three points to its left and the three points to its right) to each histogram to eliminate statistically non-significant fluctuations. As shown in Figure 1 (black line), this leads to a better determination of the location of the maximum probability (i.e., the mode). The resulting smoothed histogram is only used for estimating the mode; the rest of statistical parameters are computed from the original (not-smoothed) histogram. We compute a SMOS-based climatological value for each given 5-tuple (denoted as $sss\_clim(\varphi, \lambda, d, x, \theta)$) by averaging all the retrieved single-angle SSSs lying in a range of $\pm\sigma$ around the estimated mode, where σ is the standard deviation of the single-angle SSSs for that 5-tuple.

Figure 2 shows two maps of the SMOS-based climatologies, corresponding to ascending overpasses, $x = 0$ km, $\theta = 5°$ (top) and $\theta = 35°$ (bottom). Significant differences are found for different θ values (that is, depending on the relative position of the pixel in the ARF), see Figure 3. The differences are

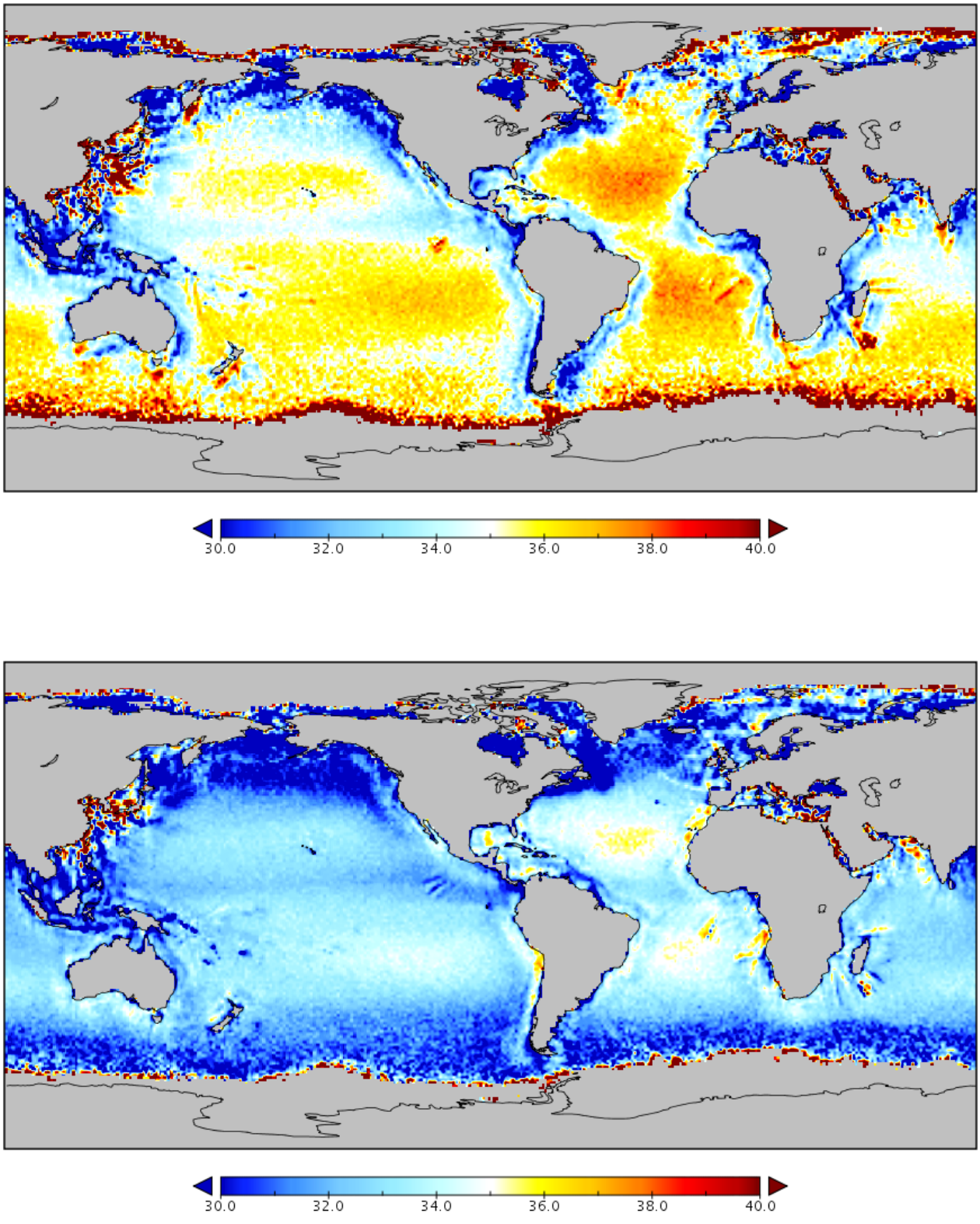

Figure 2: SMOS-based climatology for ascending overpasses and $x = 0$ km and $\theta = 5°$ (top) and $x = 0$ km and $\theta = 35°$ (bottom).

notably large close to the coast due to LSC, although they can be significant also elsewhere. A close inspection of the SMOS-based climatologies shows that for any given value of x and θ the deviation of SMOS-based climatology from a standard annual climatology is far from being spatially constant, even in open sea (see Figure 4).

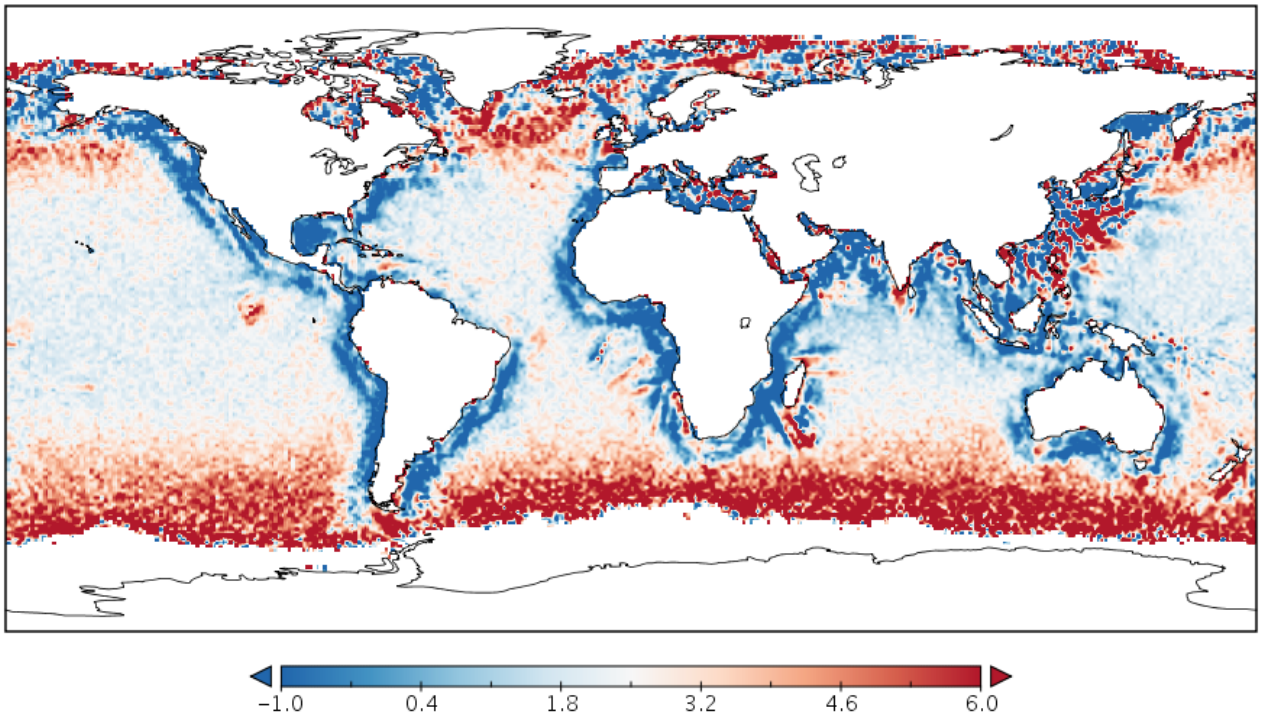

Figure 3: Map of differences between the SMOS-based climatology for ascending overpasses and x=0 km and $\theta = 5^o$ and the SMOS-based climatology for ascending overpasses and x=0 km and $\theta = 35^o$.

2.1.5 Spatial bias correction

For the generation of higher-level SSS products, single-angle SSS retrievals (Section **??**) are corrected with their corresponding SMOS-based climatological value (sss_{clim}), thus creating a set of so-called SMOS-based anomalies (sss_{an}):

$$sss_{an}(\varphi, \lambda, d, x, \theta) = SSS(\varphi, \lambda, d, x, \theta) - sss_{clim}(\varphi, \lambda, d, x, \theta). \quad (2)$$

In order to obtain an absolute value of SSS, a time-independent reference SSS value must be added to the L2 product. We use here the annual SSS climatology provided by the World Ocean Atlas 2013 (WOA2013) at $0.25^o \times 0.25^o$ (average decadal product, which is accessible at [National Oceanographic Data Center, [**?**]).

2.1.6 SSS filtering criteria for non-Bayesian approach

After computing SMOS-based climatologies, several quality control criteria are applied to discard poor quality values. For a given 5-tuple, $c = (\varphi, \lambda, d, x, \theta)$, a SMOS-climatological value is discarded (and

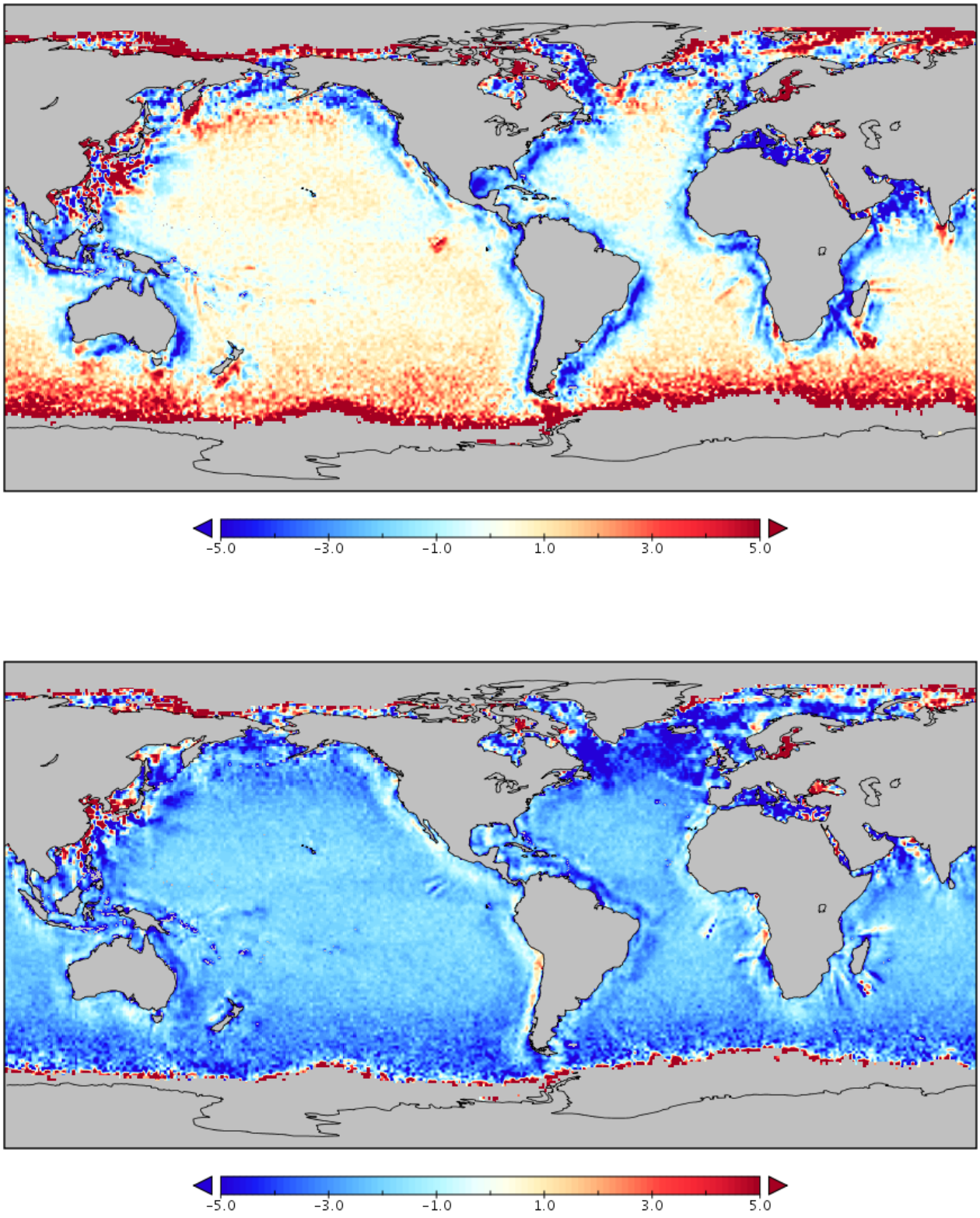

Figure 4: Difference between SMOS-based climatology and the annual WOA2013 climatology for ascending overpasses and $x = 0$ km and $\theta = 5°$ (top) and $x = 0$ km and $\theta = 35°$ (bottom).

hence all related single-angle SSS retrievals) when the associated histogram suffers from one or more of the following conditions:

- It has less than 100 measurements;
- Its standard deviation is greater than 10 psu;
- The absolute value of its normalized skewness is greater than 1;
- Its kurtosis is lower than 2

Two additional filtering criteria are applied to the SMOS-based anomalies:

- If the histogram corresponding to a given geographical and orbital coordinates $c = (\varphi, \lambda, d, x, \theta)$ has been discarded following the criteria of Section 2.1.6, then all the $sss_{an}(\varphi, \lambda, d, x, \theta)$ are also discarded.
- When the SMOS-based anomaly is greater than the standard deviation of the distribution, the value is considered an outlier and, therefore, it is also discarded.

As an example, see the two histograms displayed in Figure 1. The one in the left is accepted, as none of the conditions above is verified (it has 581 measurements, a standard deviation of 2.31, skewness equal to 0.97 and kurtosis equal to 3.74). The one in the right has 369 measurements, a standard deviation 5.82 and a 0.19 skewness, which are right, but its kurtosis (1.79) is too low and, therefore, it is discarded.

2.1.7 Temporal bias mitigation

An additional time-dependent bias correction is needed in order to mitigate the effect of seasonal and other time-dependent biases which affect the SMOS T_B ([Martín-Neira et al., 2016]). In [Olmedo et al., 2017], the authors proposed subtracting the global mean of the SMOS SSS anomaly for each 9-day map. This assumption is appropriate for global SSS maps, as it implies that the total content of salt remains constant in time. However, the application of this hypothesis regionally, in particular at high latitudes, produces seasonal biases. In other words, there are net exchanges of salinity across region boundaries. In a recent study [Olmedo et al., 2018b], a multivariate analysis is used to characterize and to mitigate the time-dependent bias in the SMOS SSS maps in the Mediterranean Sea. In this work, we include a simpler time-dependent bias correction:

- We consider the Argo SSS available for the same 9-day period used in the generation of the 9-day SMOS SSS maps.
- We compute the median of the differences between the collocated SMOS SSS fields and the Argo SSS.
- We subtract this median from each 9-day SMOS SSS map.

Figure 5 shows the time-dependent correction resulting from this procedure, which has been applied to each map.

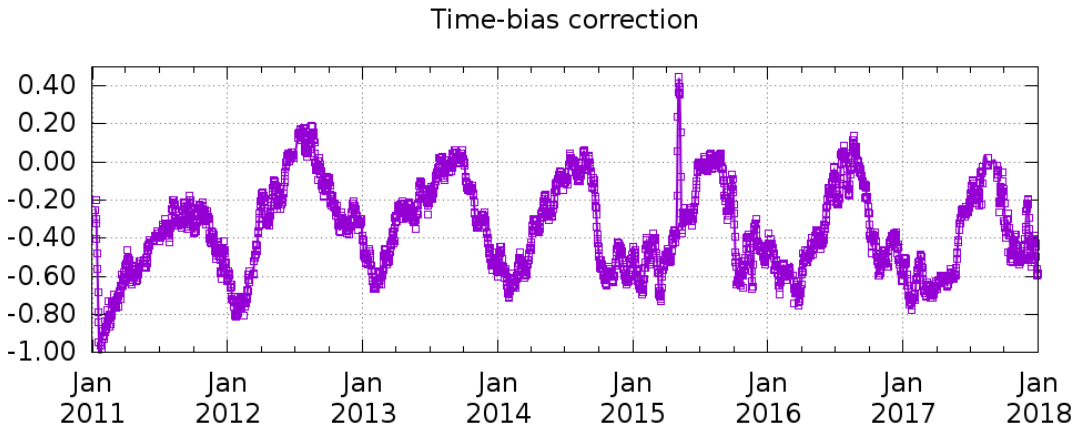

Figure 5: Time-bias correction applied to the 9-day SMOS SSS L3 maps. During the 1st-10th of January 2011 SMOS provided degraded acquisitions due to a problem in the physical temperatures acquisition (reported in *https://earth.esa.int/c/document_library/get_file?folderId=118493&name=DLFE-5407.pdf*). The reason of the jump at the end of April 2015 is still under study, but probably it is related to several degraded orbits that were reported in the data quality report (available on *https://earth.esa.int/documents/10174/1785702/SMOS_Public_Monthly_Report_April_2015*).

2.2 L3 Algorithm

L3 SSS maps are generated by means of a an objective analysis method, as presented in [Zweng et al., 2013]. The time period has been selected equal to 9 days because it corresponds to a half almost repeat subcycle of SMOS, and so it is the shortest time period providing a complete spatial coverage of all the regions. The correlation radii considered are 321, 267 and 175 km.

3 ARCTIC SSS PRODUCT

3.1 Ocean files structure

The resulting Level 3 products are distributed in netCDF format and the name of each file follows the layout:

```
BEC_AAAAAA_B_CCCCCCCCCCCCCCC_DDDDDDDDDDDDDDD_EEEEEEE_FFF_GGG.nc
BEC_EARTOA_B_20161231T000000_20170109T000000_025_002.nc
```

Where each field of the filename is as follows:

- `AAAAAA`: is the product's name:
  - `BINNED`: Binned product
  - `ADVAOA`: Advanced Optimal....
  - `OI____`: Optimal Interpolation product
  - `L4_SST`: Fused product using singularity analysis techniques derived from SST

  - EXPSST: Singularity Exponents

- B: Indicates the orbit composition of the product.
  - A for products composed by ascending orbits
  - D for products composed by descending orbits
  - B for products composed by both types of orbits

- CCCCCCCCCCCCCCC: Starting UTC time (YYYYMMDDThhmmss) of the first L2 product used to create the L3/L4 product. This is an inherited value in products not derived directly from Level 2 orbits.

- DDDDDDDDDDDDDDD: Ending UTC time (YYYYMMDDThhmmss) of the last L2 product used to create the L3/L4 product. This is an inherited value in products not derived directly from Level 2 orbits (Optimal Interpolation and L4 products).

- EEEEEEE: Internal code that designates the filtering applied. This is an inherited value in products not derived directly from Level 2 orbits.

- FFF: Grid size of the product in a lat-lon grid multiplied by 100

- GGG: Version number of the file starting at 001

3.2 Data Definition

The structure of the netCDF files with its dimensions, variables and global attributes is detailed here:

```
dimensions:
    y = 721 ;
    x = 721 ;
    time = UNLIMITED ; // (1 currently)
variables:
    int EASE_NL ;
       EASE_NL:cell_area = "25km_x_25km" ;
       EASE_NL:longitude_of_projection_origin = 0.f ;
       EASE_NL:latitude_of_projection_origin = 90.f ;
       EASE_NL:height_dimension = 721.f ;
       EASE_NL:width_dimension = 721.f ;
       EASE_NL:column_map_origin_r0 = 360.f ;
       EASE_NL:row_map_origin_s0 = 360.f ;
       EASE_NL:Minimum_longitude = -180.f ;
       EASE_NL:Maximum_longitude = 180.f ;
       EASE_NL:Minimum_latitude = -0.34f ;
       EASE_NL:Maximum_latitude = 90.f ;
       EASE_NL:reference_projection = "http://nsidc.org/data/ease/ease_grid.html"
;        EASE_NL:proj4tex = "+proj=laea +lat_0=90 +lon_0=0 +x_0=0 +y_0=0 +a=6371228
+b=6371228 +units=m +no_defs" ;
       EASE_NL:grid_mapping_name = "lambert_azimuthal_equal_area" ;
    float latitude(y, x) ;
       latitude:standard_name = "latitude" ;
       latitude:long_name = "Latitude" ;
```

```
        latitude:units = "degrees_north" ;
        latitude:valid_min = -0.34f ;
        latitude:valid_max = 90.f ;
    float longitude(y, x) ;
        longitude:standard_name = "longitude" ;
        longitude:units = "degrees_east" ;
        longitude:long_name = "Longitude" ;
        longitude:valid_min = -180.f ;
        longitude:valid_max = 180.f ;
    float oa_sss(time, y, x) ;
        oa_sss:missing_value = -999.f ;
        oa_sss:_FillValue = -999.f ;
        oa_sss:standard_name = "sea_surface_salinity" ;
        oa_sss:long_name = "Sea Surface Salinity" ;
        oa_sss:valid_min = 0.f ;
        oa_sss:valid_max = 50.f ;
        oa_sss:grid_mapping = "EASE_NL" ;
        oa_sss:coordinates = "time longitude latitude" ;
        oa_sss:units = "1" ;
        oa_sss:description = "Sea Surface Salinity objectively analized using
debiased non-Bayesian retrieval [psu]" ;
    int time(time) ;
        time:standard_name = "time" ;
        time:long_name = "time" ;
        time:units = "seconds since 1970-1-1 00:00:00" ;
        time:time = "t" ;
        time:coordinate_defines = "center" ;
        time:_CoordinateAxisType = "Time" ;
        time:calendar = "gregorian" ;
global attributes:
    :date_created = "2018-02-26 08:41:22 GMT" ;
    :time_coverage_start = "2016-04-02T01:55:08" ;
    :time_coverage_end = "2016-04-10T23:24:45" ;
    :geospatial_lon_units = "degrees_east" ;
    :geospatial_lat_units = "degrees_north" ;
    :geospatial_lon_min = -179.875f ;
    :geospatial_lon_max = 179.875f ;
    :geospatial_lat_min = -89.875f ;
    :geospatial_lat_max = 89.875f ;
    :institution = "SMOS Barcelona Expert Centre, ICM-CSIC / UPC, Barcelona,
Spain" ;
    :copyright = "BEC research products are freely distributed.  SSS have been
retrieved following the algorithm described in Olmedo, E. et al., De-biased
non-Bayesian Retrieval:  a novel approach to SMOS Sea Surface Salinity, Remote
Sensing of Environment 193 (2017) 103126.  The complete description of the
methodology as well as the analysis of the quality assessment of the product
can be found in Olmedo, E. et al., Seven Years of SMOS Sea Surface Salinity
at High Latitudes:  Variability in Arctic and Sub-Arctic Regions, Remote Sensing,
2018, 10(11).  If this data is used for publication, the following ackowlegment
```

should be included: These data were produced by the Barcelona Expert Centre (http://bec.icm.csic.es/). The Barcelona Expert Center is a joint initiative of the Spanish Research Council (CSIC) and Technical (University of Catalonia (UPC), mainly founded by the Spanish National Program on Space." ;
:references = "Olmedo, E. et al., Seven Years of SMOS Sea Surface Salinity at High Latitudes: Variability in Arctic and Sub-Arctic Regions, Remote Sensing, 2018, 10(11), 1772; doi:10.3390/rs10111772" ;
:title = "Arctic Sea Surface Salinity L3 map" ;
:Conventions = "CF-1.6" ;

3.3 Data Access

The Arctic SMOS SSS v2.0 produced at BEC is freely available through a SFTP server. If your browser is SFTP compatible you can browse directly from sftp://becftp.icm.csic.es:27500 address. The data can be download after completing registration in our BEC ftp service (http://bec.icm.csic.es/bec-ftp-service-registration/). For more information about the BEC ftp service, please visit http://bec.icm.csic.es/bec-ftp-service/. For any further assistance, contact to smos-bec@icm.csic.es.

The following diagram tree shows the complete path to the Arctic SMOS SSS v2.0 repository.

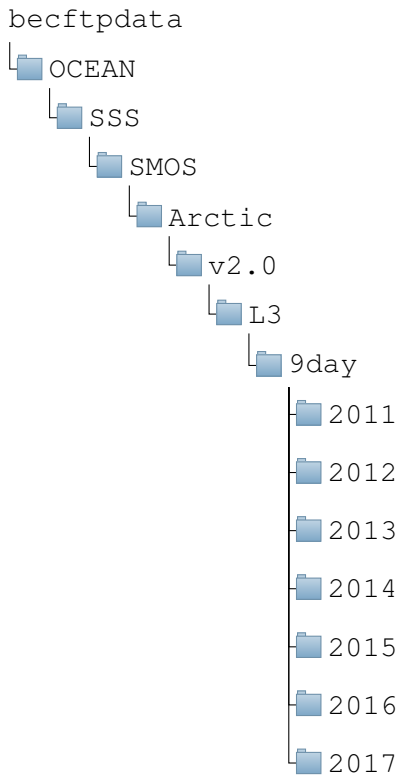

A QUALITY ASSESSMENT

A.1 Datasets

The quality of SSS SMOS is assessed using different datasets that are briefly described hereafter.

A.1.1 TARA salinity

The Tara Polar Circle Expedition data set (hereafter TARA SSS) ([Reverdin et al., 2014]) is used to validate the SMOS 9-day maps in the Arctic. This campaign took place in the Arctic Ocean from June to October 2013, and a thermosalinograph (TSG) Seabird SB45 and a temperature sensor (SBE38) recorded sea surface temperature and salinity at 3 m depth during the whole cruise. Since TARA salinity data presents a large range of spatial variability in the Arctic Ocean ($\approx$ 26 to 35), it becomes a very valuable source for assessing the annual SSS reference used for the generation of the SMOS SSS product.

The collocation strategy between satellite and TARA SSS is the following: a given value of TARA SSS acquired at time instant t_0 is compared with the 9-day SMOS SSS map centered around t_0. All the TARA SSS that cross a single SMOS cell (25×25 km) are averaged and the resulting mean value is the one that is compared with the SMOS SSS. In Figure 6 (top-right) the TARA SSS measured in the expedition are represented.

A.1.2 Argo salinity

We use Argo salinity [Argo, 2000] in section 2 for the characterization of the SMOS SSS bias and for the generation of a time-dependent bias correction. After that, Argo data is also compared with the resulting SMOS products in section A.3.

We consider the uppermost salinity measurement provided by the Argo profiles (hereafter Argo SSS) to be compared with the 9-day SMOS SSS maps. Such that, for every SMOS SSS 9-day map, the available Argo SSS during these 9 days are compared with the corresponding fields of the SMOS SSS map. The cut-off depth for Argo profiles is taken at 10 m, but no measurements shallower than 0.5 m are used due to the formation of bubbles and foam. In the case of SOLO and PROVOR Argo floats, only the data deeper than 5 m bellow are used because their Conductivity, Temperature and Depth (CTD) probes stop pumping water at around 5 m bellow the surface. Profiles from BioArgo and those included in the greylist (i.e. floats which may have problems with one or more sensors) are discarded. In addition we use World Ocean Atlas (WOA) 2013 as an indicator: Argo float profiles with anomalies larger than 10^oC in temperature or 5 PSU in salinity when compared to WOA are discarded. Only profiles having temperature close to surface between -2.5 and 40^oC and salinity between 2 and 41 PSU are used. In Figure 6 (top-left) the number of Argo SSS and their spatial distribution for the period of study is represented.

A.1.3 TSG salinity data

We use 86 transects provided by Copernicus (hereafter TSG SSS) for assessing the SMOS SSS. This data is freely available on *http://marine.copernicus.eu/services-portfolio/access-to-products/* and it is labeled as *INSITU_ARC_NRT_OBSERVATIONS_013_031*. In Figure 6 (bottom-left), the locations of the measurements is shown. The collocation strategy between SMOS and TSG SSS is the same than that of SMOS and TARA. Only TSG SSS data flagged as "good quality" have been used. Measurements deeper than 10 m are discarded. In section A.4, this data set is used as an independent

reference for the SMOS SSS validation.

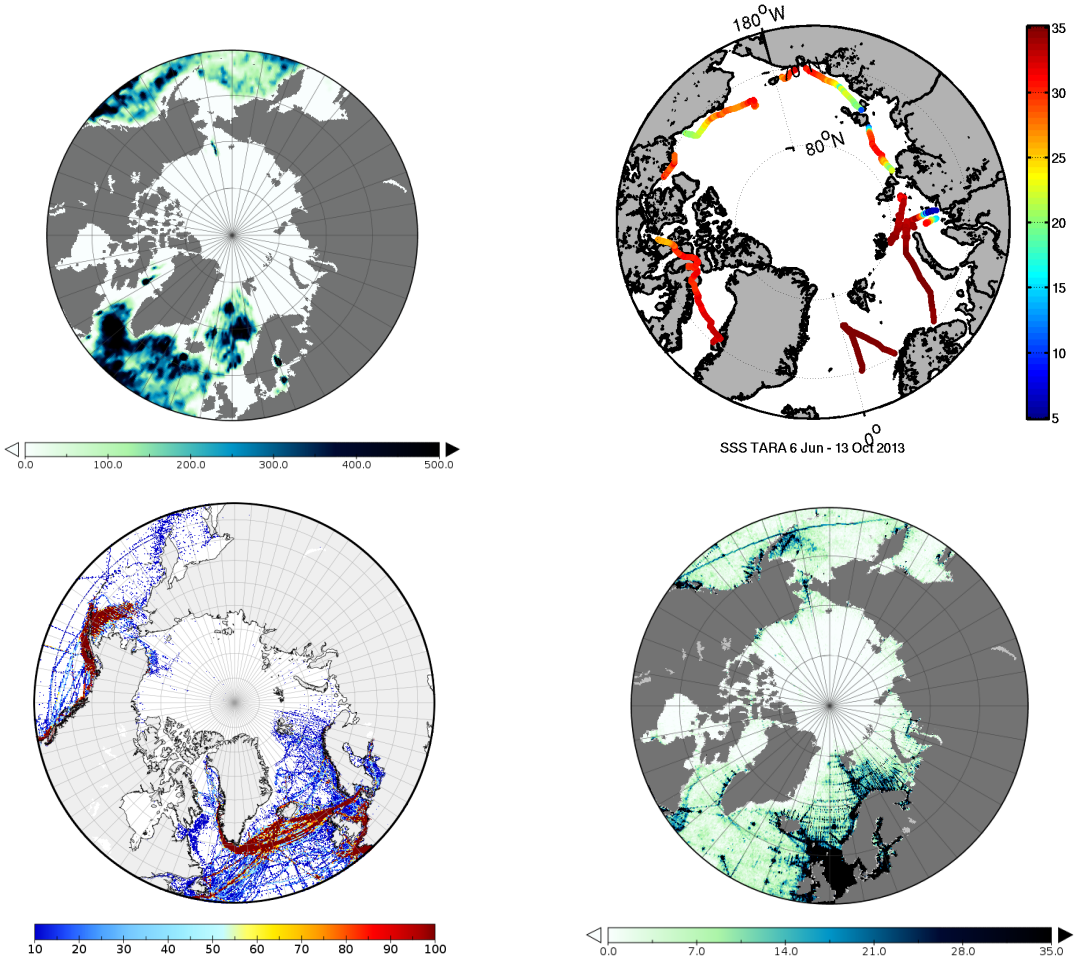

Figure 6: Number of measurements provided by Argo floats in the period of study 2011-2017 (top-left), salinity values provided in the TARA campaign (top-right), number of SSS measurements provided by the TSG that have been used in this study for validation (bottom-left) and number of in situ measurements used in the computation of annual SSS climatology WOA (bottom-right).

A.2 Comparison with TARA SSS: impact analysis of the SSS annual reference

The validation against TARA SSS is done by separating the transects per different seas, for a better understanding of the regional quality of the SMOS SSS product. We divide the whole data set into 6 regions: Norwegian Sea, Barents Sea, Laptev Sea, East Siberian Sea, Chukchi Sea and Baffin Bay. Table 1 shows the statistics of the comparison between SMOS SSS and TARA. For a more detailed analysis the reader is refer to section 4.1 of [Olmedo et al., 2018a].

A.3 Comparison with Argo SSS

In this section, a statistical comparison between the 9-day SMOS SSS products and salinity provided by Argo floats (see section A.1.2) is presented.This data set is not an independent source of SSS data for assessing the global mean of the product since it is used for performing the time-dependent bias

Table 1: Statistics in the comparison of SMOS SSS with TARA SSS

Arctic Region	SMOS - TARA			
	mean	std	RMS	R
Norwegian sea	0.11	0.15	0.18	0.73
Baffin Bay	0.16	0.46	0.49	0.51
Chukchi region	2.16	2.18	3.07	0.91
Barents sea	-1.35	1.37	1.93	0.88
Laptev sea	1.37	3.48	3.74	0.68
Siberian region	-3.20	2.50	4.06	0.8

correction (see section 2). However, this comparison is used to assess the residual spatial biases and the uncertainty (standard deviation of the differences SMOS-Argo SSS) of the SMOS SSS product.

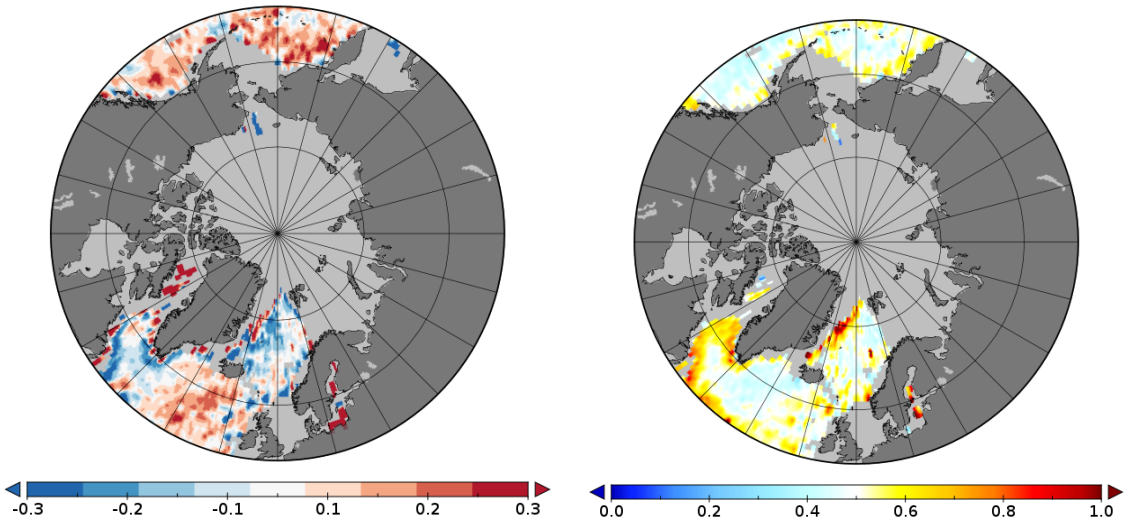

Figure 7: Spatial distributions of the differences between SMOS and Argo SSS. Left: the mean of SMOS-Argo SSS; right: the std of the difference.

In Figure 7 the mean of the differences between SMOS and Argo SSS during 2011-2017 are displayed (left), as well as the standard deviation of these differences (right). Large differences are observed in the Baffin Bay, the Labrador Sea and the eastern coast of Greenland (Greenland sea and Fram Strait). A possible factor contributing to these differences is the high-frequency and small-scale variability of SSS associated with the currents and the differences in temporal and spatial samplings between SMOS and the Argo SSS. SMOS maps are based on 9-day averages while Argo SSS represents instantaneous salinity values. Besides, SMOS SSS provides spatial average within a 40-km footprint, further smoothed by the Objective Analysis large correlation radii (see section 2), while in situ data are instantaneous and point-wise measurements. The differences caused by these effects could be substantial if there are significant sub-footprint variability [Boutin et al., 2016].

The northern coast of Alaska also presents large discrepancies between SMOS and Argo SSS. This region is strongly stratified, and the mixed layer is typically thinner than 3 m in this region. This implies also a limitation in the comparison of SMOS with Argo data since SMOS is measuring the first cm depth and Argo SSS are typically provided at some meters depth.

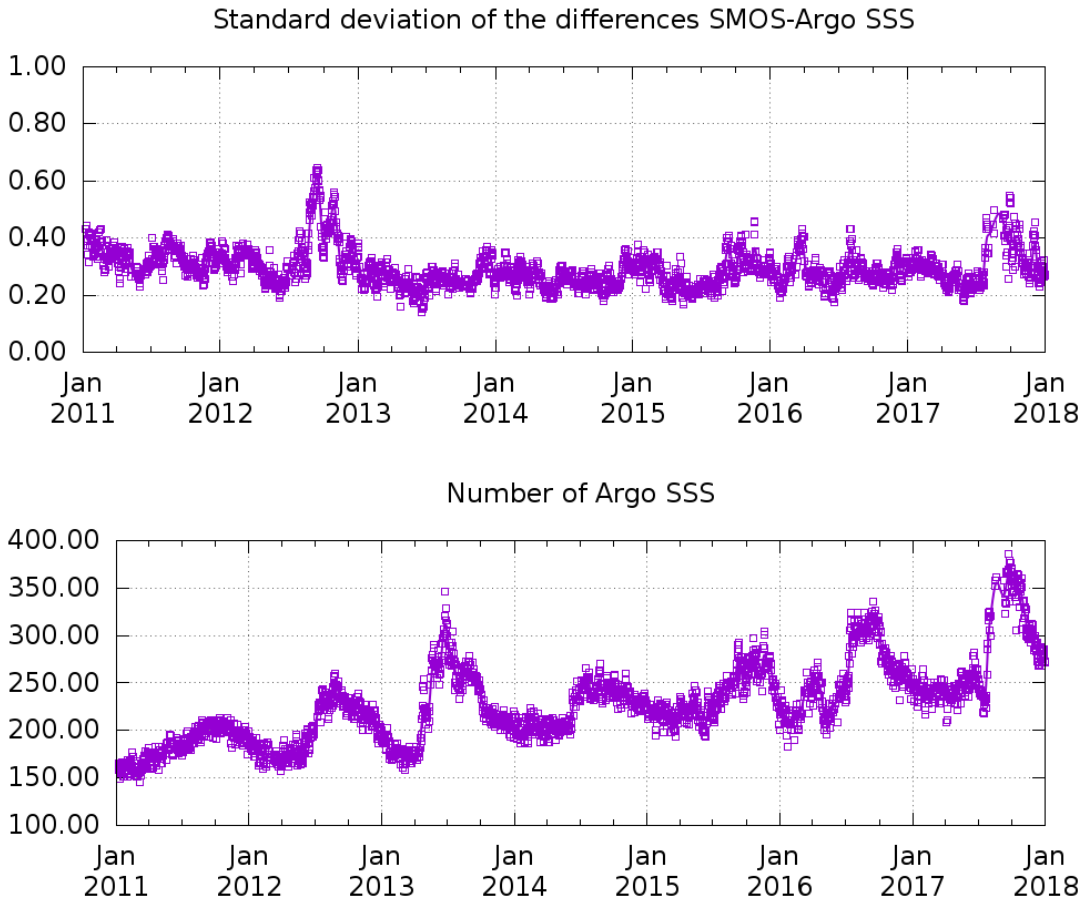

Figure 8: Time evolution of the standard deviation of the differences between SMOS and Argo SSS (top) and the number of measurements used in the comparison (bottom). The statistics are computed for data above 50^{o}N. Every SMOS 9-day map is compared with the Argo SSS available for the same 9-day period.

Figure 8 shows temporal evolution of the the standard deviation of the differences SMOS-Argo SSS (top) and the number of collocations used in the statistics (bottom). Such that, for a given time t (x-axis), the point represents the std of the differences between SMOS and Argo SSS and the number of collocations, respectively, for all the collocations available with t the first day of the 9-day period. We do not show the time evolution of the mean difference SMOS - Argo SSS, because by definition (see section 2) is zero since the seasonal bias that was present in the previous version of this product has been mitigated. Large std values are observed in autumn 2012. The causes for such large std values (whether geophysical or instrumental) are currently being investigated. Our preliminary hypothesis indicates that they are due to a strong RFI episode. The std of the differences between SMOS and Argo SSS is between 0.2 psu and 0.35 psu.

Table 2: Regional analysis on the differences between TSG and SMOS SSS (SMOS-TSG). Regional statistics of differences between SMOS and ARGO are also included.

Region	Latitude Range	Longitude Rage	SMOS - TSG			SMOS - ARGO		
			meas	mean	std	meas	mean	std
Denmark Strait	60N - 65N	40W - 25W	2322	0.22	0.28	25153	0.02	0.21
North Atlantic	50N-60N	50W - 20W	8028	0.19	0.45	102575	0.01	0.35
Norwegian Sea	60N - 70N	10W - 5E	4587	0.02	0.67	33841	-0.05	0.31
Northern Sea	55N - 60N	0E- 5E	53366	0.16	0.99	0	-	-
Gulf of Alaska	55N-60N	175W-125W	604	0.26	0.72	14841	0.09	0.27
Chuckchi Sea	70N - 75N	170W - 145W	315	0.01	1.42	1751	-0.99	0.37
Labrador Sea	55N - 60N	55W - 45W	737	0.14	0.71	33711	-0.07	0.29
Baffin Bay	60N - 65N	65W - 55W	278	0.89	0.62	5919	-0.02	0.41

A.4 Comparison with TSG data from Copernicus

In this section we compare SMOS SSS with SSS provided by 86 TSG transects distributed by Copernicus. The objective is to show that both SSS sources agree on the major features of the inter annual SSS dynamics, despite the different spatial and temporal resolutions of TSG and SMOS data. The statistics of the differences between SMOS and TSG SSS in several regions are provided in Table 2. In general, SMOS SSS has a positive bias with respect to TSG SSS and larger standard deviation than the standard deviations resulting from the comparison with ARGO. Part of the increase in the standard deviation can be explained because the TSG SSS data reaches more coastal regions than Argo data do. Typically, these coastal regions are affected by complex circulation dynamics that could form filaments and mesoscale and submesoscale structures with strong SSS gradients and fast dynamics that can not be resolved by SMOS, particularly after applying objective analysis. In those regions, we typically observe that the TSG captures strong SSS gradients with differences between consecutive coastal pixels greater than several PSU. More detailed discussions of the results shown in Table 2 are provided in section 4.3 of [Olmedo et al., 2018a].

References

[Argo, 2000] Argo (2000). Argo float data and metadata from global data assembly centre (argo gdac). *SEANOE, http://doi.org/10.17882/42182*.

[Boutin et al., 2016] Boutin, J., Chao, Y., Asher, W. E., Delcroix, T., Drucker, R., Drushka, K., Kolodziejczyk, N., Lee, T., Reul, N., Reverdin, G., Schanze, J., Soloviev, A., Yu, L., Anderson, J., Brucker, L., Dinnat, E., Santos-Garcia, A., Jones, W. L., Maes, C., Meissner, T., Tang, W., Vinogradova, N., and Ward, B. (2016). Satellite and in situ salinity: Understanding near-surface stratification and subfootprint variability. *Bulletin of the American Meteorological Society*, 97(8):1391–1407.

[Deimos, 2014] Deimos (2014). *SMOS L1 Processor L1C Data Prorocessing Model. SO-DS-DME-L1PP-0009*. Deimos. version 2.14.

[ESA, 2014] ESA (2014). Earth Observation CFI v3.x branch. http://eop-cfi.esa.int/index.php/mission-cfi-software/eocfi-software/branch-3-x. [Online; accessed 23-August-2016].

[Guimbard et al., 2012] Guimbard, S., Gourrion, J., Portabella, M., Turiel, A., Gabarro, C., and Font, J. (2012). SMOS Semi-Empirical Ocean Forward Model Adjustment. *Geoscience and Remote Sensing, IEEE Transactions on*, 50(5):1676 –1687.

[Martín-Neira et al., 2016] Martín-Neira, M., Oliva, R., Corbella, I., Torres, F., Duffo, N., Duran, I., Kainulainen, J., Closa, A., Zurita, A., Cabot, F., Khazaal, A., Anterrieau, E., Barbosa, J., Lopes, G., Tenerelli, J., Diez-Garcia, R., Fauste, J., Martin-Porqueras, F., González-Gambau, V., Turiel, A., Delwart, S., Crapolicchio, R., and Suess, M. (2016). SMOS Instrument performance and calibration after six years in orbit. *Remote Sensing of Environment*, 180:19–39.

[McMullan et al., 2008] McMullan, K., Brown, M., Martin-Neira, M., Rits, W., Ekholm, S., Marti, J., and Lemanczyk, J. (2008). Smos: The payload. *Geoscience and Remote Sensing, IEEE Transactions on*, 46(3):594 –605.

[Meissner and Wentz, 2004] Meissner, T. and Wentz, F. (2004). The complex dielectric constant of pure and sea water from microwave satellite observations. *Geoscience and Remote Sensing, IEEE Transactions on*, 42(9):1836–1849.

[National Oceanographic Data Center, 2013] National Oceanographic Data Center (2013). WOA 2013 V2 Data Access. https://www.nodc.noaa.gov/cgi-bin/OC5/woa13/woa13.pl. [Online; accessed 23-August-2016].

[Olmedo et al., 2018a] Olmedo, E., Gabarró, C., González-Gambau, V., Martínez, J., Ballabrera-Poy, J., Turiel, A., Portabella, M., Fournier, S., and Lee, T. (2018a). Seven years of smos sea surface salinity at high latitudes: Variability in arctic and sub-arctic regions. *Remote Sensing*, 10(11).

[Olmedo et al., 2017] Olmedo, E., Martinez, J., Turiel, A., Ballabrera-Poy, J., and Portabella, M. (2017). Debiased non-Bayesian retrieval: a novel approach to SMOS Sea Surface Salinity. *Remote sensing of Environment*, 193(Supplement C):103–126.

[Olmedo et al., 2018b] Olmedo, E., Taupier-Letage, I., Turiel, A., and Alvera-Azcárate, A. (2018b). Improving SMOS Sea Surface Salinity in the Western Mediterranean Sea through Multivariate and Multifractal Analysis. *Remote sensing*, 10(3)(485).

[Reul et al., 2007] Reul, N., Tenerelli, J., Guimbard, S., Collard, F., Kerbaol, V., Skou, N., Cardellach, E., Tauriainen, S., Bouzinac, C., Wursteisen, P., Tournadre, J., and Chapron, B. (2007). Analysis of L-band radiometric measurements conducted over the North Sea during the CoSMOS-OS airborne campaign. *IEEE International Geoscience and Remote Sensing Symposium, IGARSS2007*.

[Reverdin et al., 2014] Reverdin, G., Le Goff, H., Tara Oceans Consortium, C., and Tara Oceans Expedition, P. (2014). Properties of seawater from a Sea-Bird TSG temperature and conductivity sensor mounted on the continuous surface water sampling system during campaign TARA_20090913Z of the Tara Oceans expedition 2009-2013.

[Tenerelli et al., 2008] Tenerelli, J., Reul, N., Mouche, A., and Chapron, B. (2008). Earth-viewing L-band radiometer sensing of sea surface scattered celestial sky radiation - part I: general characteristics. *IEEE T. Geoscience and Remote Sensing*, 46(3):659–674.

[Zweng et al., 2013] Zweng, M., Reagan, J., Antonov, J., Locarnini, R., Mishonov, A., Boyer, T., Garcia, H., Baranova, O., Johnson, D., Seidov, D., and Biddle, M. (2013). *World Ocean Atlas 2013, Volume 2: Salinity*. Levitus, Ed., A. Mishonov Technical Ed.; NOAA Atlas NESDIS 74, 39 pp.